Microbiology and Infectious Disease
Computational and Systems Biology

An antimicrobial drug recommender system using MALDI-TOF MS and dual-branch neural networks

Reviewed Preprint
v2 • September 3, 2024
Revised by authors

Reviewed Preprint
v1 • May 1, 2024

Gaetan De Waele ✉, **Gerben Menschaert, Willem Waegeman**

Ghent University, Ghent, Belgium

Abstract

Timely and effective use of antimicrobial drugs can improve patient outcomes, as well as help safeguard against resistance development. Matrix-assisted laser desorption/ionization time-of-flight mass spectrometry (MALDI-TOF MS) is currently routinely used in clinical diagnostics for rapid species identification. Mining additional data from said spectra in the form of antimicrobial resistance (AMR) profiles is, therefore, highly promising. Such AMR profiles could serve as a drop-in solution for drastically improving treatment efficiency, effectiveness, and costs.

This study endeavours to develop the first machine learning models capable of predicting AMR profiles for the whole repertoire of species and drugs encountered in clinical microbiology. The resulting models can be interpreted as drug recommender systems for infectious diseases. We find that our dual-branch method delivers considerably higher performance compared to previous approaches. In addition, experiments show that the models can be efficiently fine-tuned to data from other clinical laboratories. MALDI-TOF-based AMR recommender systems can, hence, greatly extend the value of MALDI-TOF MS for clinical diagnostics.

All code supporting this study is distributed on PyPI and is packaged under: https://github.com/gdewael/maldi-nn

eLife assessment

This **valuable** study presents a machine learning model to recommend effective antimicrobial drugs from patients' samples analysed with mass spectrometry. The evidence supporting the claims of the authors is **convincing**, although including a measure of statistical significance to compare different proposed models would further strengthen the support. This work will be of interest to computational biologists, microbiologists, and clinicians.

https://doi.org/10.7554/eLife.93242.2.sa3

1. Introduction

In diagnostic laboratories, matrix-assisted laser desorption/ionization time-of-flight mass spectrometry (MALDI-TOF MS) is routinely used for microbial species identification (Hou et al., 2019). Usually, microbial samples only require an overnight culturing step before being analyzed with mass spectrometry (Van Veen et al., 2010; Cuénod et al., 2021). Consequently, the technology provides a timeand costefficient way to accurately identify the pathogen underlying an infection.

Due to the rapid evolution of antibiotic resistant strains, it is increasingly difficult to determine a treatment based on only species identity. It has been estimated that infections caused by antibiotic-resistant bacteria have caused the deaths of 1.27 million people in 2019, making AMR one of the leading causes of death on earth (Murray et al., 2022). Projections have estimated that this annual number could rise to 10 million by 2050 (O'Neill, 2016), highlighting the need for responsible antimicrobial drug use. In light of this, diagnostic laboratories will often perform various tests, such as dilution arrays or disc diffusion tests, to probe which drug will be effective (Khan et al., 2019). Such experiments typically require further culturing and are either costly, labor-intensive, time-intensive, or a mixture of the above (Humphries, 2022).

Given that MALDI-TOF spectra are already routinely used for identification, it is worth investigating to which extent they can contain further information regarding the resistance status of strains (Weis et al., 2020a). Mining this information from the spectra could help inform healthcare workers of candidate drugs. This may nullify the need for phenotypical experiments, or (at least) direct the tests by narrowing down the choices. Furthermore, possessing a detailed resistance profile allows to treat with more specifically-working drugs (instead of broadspectrum antibiotics) (Weis et al., 2022). Consequently, predicting resistance status from MALDI-TOF spectra could help towards the goals of antibiotic stewardship (Shlaes et al., 1997).

It has been described that some known resistance mechanisms are outside of the m/z range that MALDI-TOF spectrometers can accurately measure (Humphries, 2022). Still, it remains largely unknown to which extent co-evolved traits, such as subtle changes in metabolism caused by the resistance mechanism, can be detected by MALDI-TOF spectra. A number of studies have shown that some resistant strains can reliably be predicted from MALDI-TOF MS, either by identifying and detecting specific markers (e.g. peaks) or by learning patterns from data (see §2.1). To our knowledge, all of these studies have modeled AMR prediction for specific species-drug combinations. For this reason, they learn very specific markers of resistance, not guaranteed to extrapolate well to other drugs and species. As susceptibility rapidly evolves, it is practically impossible to perform such studies for all clinically-relevant species-drug combinations. As such, the value of aforementioned studies remains of exploratory nature with limited practical value. In addition, their performance remains limited owing to small sample sizes and, likely, the inability of MALDI-TOF spectra to fully discriminate between the characteristics of interest (Bai et al., 2017). The recently published DRIAMS dataset (Weis et al., 2022) contains phenotypic AMR data covering a wide range of species and drugs, allowing to study MALDI-TOF-based AMR prediction on an unprecedented scale.

We posit that the most pertinent challenge healthcare workers face regarding AMR is to choose between all possible drugs given an infection, not whether one specific drug will be effective or not. For this reason, we argue that our models and evaluation metrics should be designed to optimally answer that question. In this study, a recommender model is proposed that can predict AMR for the whole range of pathogens and drugs encountered in clinical microbiology. In addition, species-specific recommender models for a range of common species are also trained. Our method jointly learns representations for antibiotic drugs and bacterial MALDITOF spectra. It

can be used to recommend the mostlikely drug to work for any drug-spectrum combination. Consequently, the model is broadly-applicable and practical to use. To summarize, our contributions are as follows:

1. We formulate a dual-branch neural network recommender system for the prediction of AMR profiles. The model operates on MALDI-TOF spectra, as well as a representation of the candidate drug.
2. We evaluate multiple state-of-the-art techniques for representing drug identity in the model.
3. We compare "general" recommenders (trained on all spectra from all species) against speciesspecific recommender models
4. We perform evaluations by comparing our methods to non-recommender system baselines.
5. We show that the model efficiently transfers to data from diagnostic laboratories it wasn't trained on. Making the model easy to adopt for hospitals lacking the means and/or volume to collect large data.

2. Related Work

2.1 MALDI-TOF-based machine learning

The most canonical task for MALDI-TOF-based methods is species identification. Identification solutions are usually provided by the MS manufacturers and are built on large, proprietary, in-house databases (Van Belkum et al., 2012). It is unclear how these closed-source identification pipelines work, but it is likely that query spectra are directly compared to the in-house database in an approach akin to nearest neighbors (Dauwalder et al., 2023). While this approach works excellently for identification of most species, some strains remain problematic (Cao et al., 2018; Vrioni et al., 2018). Furthermore, by presumably focusing on the presence or absence of specific peaks, a lot of spectral information stands unused (Florio et al., 2018).

For various difficult prediction cases, such as strain typing, researchers often resort to machine learning (Hettick et al., 2006; Wang et al., 2018; De Bruyne et al., 2011). Stifled by a historical lack of large open data, machine learning research on MALDI-TOF data remains in its infancy. Most studies have narrow scopes and simple datasets (e.g. binary classification), only warranting standard preprocessing and off-the-shelf learning techniques (Yu et al., 2022; Zhang et al., 2023; Chung et al., 2023). Only a handful of examples exist of more advanced learning techniques specifically adapted to a MALDI-TOF-based task (Mortier et al., 2021; Weis et al., 2020a; Vervier et al., 2015). For a more thorough overview of MALDI-TOF-based machine learning, readers are referred to the review of Weis et al. (2020b).

During peer-review, our attention was brought to a similar concurrent study by Visonà et al. (2023). Their study similarly shows that recommender systems-like models outperform more-narrowly trained singlespecies and single-drug models. Their analysis, however, remains limited to fingerprint-based molecular representations. In addition, in this work, we demonstrate transfer learning between hospitals.

2.2 Dual-branch neural networks

The idea of processing and combining two separate streams of information with two neural networks is applied in many fields of machine learning, collectively referred to as deep multi-target prediction (Waegeman et al., 2019; Iliadis et al., 2022).

In collaborative filtering, the goal is to predict the preference of a user to items (He et al., 2017). In its most elementary neural form, both users and items are represented by one-hot encodings, generating a model unable to make salient predictions for new users or items without having seen them during training. To solve this, a body of works exists on trying to communicate userand item-identity to the model via side-information encoded in features (Zheng et al., 2017).

Dual-branch neural networks are also prevalent in language and vision. Recent advances in (multimodal) contrastive learning of image (and text) representations often rely on two neural encoders to learn a matching score between two views of the same or discordant objects (Radford et al., 2021; Chen et al., 2020). Language retrieval systems typically compare input vectors with a database of key vectors, each derived from a neural network, using approximate nearest neighbor search techniques (Karpukhin et al., 2020). In biology, fields of research employing dualbranch neural networks include (1) drug-target interaction (Lee et al., 2019), (2) single-cell multi-omics analysis (Lance et al., 2022), and (3) transcription factor binding prediction (Yang et al., 2020), among countless others.

Most of these applications can, to varying extents, be interpreted as (collaborative filtering) recommender systems. For example, contrastive languageimage models have been used to retrieve the mostsemantically similar images to a piece of text (Beaumont, 2022).

3. Methods

3.1 Data

To train models, we use the recently published DRIAMS database, consisting of 765 048 AMR measurements derived from 55 773 spectra across four different hospitals, spanning in total 74 different drugs (Weis et al., 2022; These figures reflect the size of the dataset as downloaded from the original Dryad repository *https://doi.org/10.5061/dryad.bzkh1899q*, and after processing. For example, the number of spectra listed here corresponds to all spectra in DRIAMS for which there exists at least one AMR measurement. The total number of spectra in DRIAMS counts 250 070, but no labels are associated with these extra spectra. Further, the naming of drugs was further preprocessed such that every drug can be linked to a single chemical identifier. For more information on which drugs were merged and how this was performed, see Appendix A). Every drug is characterized by a canonical SMILES string obtained from PubChem (Kim et al., 2023). As in the original DRIAMS publication, AMR measurements are binarized according to the EUCAST norms per drug. Specifically, intermediate or resistant values are assigned a positive label, and susceptible samples a negative one. Furthermore, spectra are identically processed as in the original publication. Briefly, the following steps are performed: (1) square-root transformation of the intensities, (2) smoothing using a Savitzky-Golay filter with half-window size of 10, (3) baseline correction using 20 iterations of the SNIP algorithm, (4) trimming to the 2000-20000 Da range, (5) intensity calibration so that the total intensity sums to 1, and (6) binning the intensities by summing all values in intervals of 3 Da. After preprocessing, every spectrum is represented as a 6000-dimensional vector.

The main experiments concern models that are trained on data from one hospital only (DRIAMS-A, University Hospital Basel). All spectra and measurements derived from the other three hospitals in DRIAMS are left out for transfer learning experiments (see §4.4). Within DRIAMS-A, all spectra from before 2018 are allocated to the training set, and all spectra measured during 2018 are evenly split between validation and test set. This split in time reflects a realistic evaluation scenario, as models trained on historical data need to generalize to new patients possibly infected by newly-evolved strains. The final sizes of all splits are as follows: 409 395 labels across 28 331 spectra for the training set, 76 431 labels across 4 994 spectra for the validation set, and 76 133 labels across 4 999 spectra for the test set.

3.2 Metrics

The main objective of this study is to train models to effectively recommend treatments for patients. Hence, unless otherwise noted, metrics are computed on a per-patient basis, and then averaged. This is equivalent to macro-averaged metrics, but then computed per instance (spectrum), instead of per class (drug) (Waegeman et al., 2018). For simplicity, we omit the "macro" prefix from metrics, and unless otherwise indicated - always use spectrum-macro metrics.

The area under the receiver operating character- istic curve (ROC-AUC) measures the probability that any positive (resistant or intermediate) sample is assigned a higher predicted probability of being positive as compared to any negative (susceptible) sample. It is a measure of the average quality of the ranking of suggested drugs to a patient.

The Precision at 1 of the negative class (Prec@1(-)) evaluates how often the top-ranked prediction is correct. Hence, in this case, it reports the proportion of cases for which the "most-likely susceptible drug" prediction is actually an effective one. In a scenario where the top recommended drug is always administered, it corresponds to the percentage of correctlysuggested treatments.

3.3 Model architecture

We formulate AMR prediction as a multi-target classification problem with side-information for both instances and targets, also referred to as dyadic prediction (Waegeman et al., 2019). In this context, let us denote a sample in the dataset D by a triplet s_i, d_j, y_{ij}, where y_{ij} denotes the resistance label of a microbial spectrum $s_{i \in \{1,\ldots,n\}}$ w.r.t. a drug $d_{j \in \{1,\ldots,m\}}$. This dataset can be arranged in an incomplete score matrix$Y \in \{0,1\}^{n \times m}$. In what follows, the final architectural set-ups used to present the results are described. For details on hyperparameter tuning, readers are referred to Appendix B.

The model consists of two separate neural network embedders $E_s(\cdot)$ and $E_d(\cdot)$ for processing the spectra and drugs, respectively. The resulting instance and target embeddings x_i and t_j are then combined into a single score by their scaled dot product $\hat{y} = \frac{x_i \cdot t_j}{\sqrt{h}}$ (Rendle et al., 2020). The scaling factor $\sqrt{h}$, with h the dimensionality of both embeddings, is inspired by the formulation of self-attention (Vaswani et al., 2017). It ensures the dot products to be of manageable magnitudes, even for large values of h. This score can be used together with the sigmoid function and the crossentropy loss to optimize the two-branch neural network to map a spectrum-drug pair to a resistance label (Iliadis et al., 2022). An overview of the model is visualized in **Figure 1**.

The representations of the instance vectors x_i are extracted from a neural network $E_s(\cdot)$operating on the processed and binned MALDI-TOF spectra s_i. $E_s(\cdot)$ is parameterized by a multi-layer perceptron (MLP), consisting of a series of fully-connected layers. Between every two such layers, a series of operations consisting of (1) a GeLU activation (Hendrycks and Gimpel, 2016), (2) a dropout rate of 0.2 (Srivastava et al., 2014), and (3) layer normalization (Ba et al., 2016), is applied. We include multiple model sizes in our final results (**Table 1**). To make comparisons easier, all models output the same number of hidden dimensions that are used in the dot product, $x_i \in \mathbb{R}^{64}$.

Drug identity can be communicated to the model in a number of ways. In this work, we study the following different input representations d_j and embedder $E_d(\cdot)$ combinations:

1. As indices in a one-hot encoding paired with a single linear layer.
2. As Extended Connectivity Fingerprints paired with a single linear layer.

Figure 1.

Architectural overview of the proposed model. AMR labels of spectrum-drug pairs can be represented in an incomplete matrix. A microbial sample that is susceptible to a drug is denoted by a negative label (orange), whereas positive labels (blue) signify an intermediate or resistant combination. Instance (spectrum) and target (drug) embeddings x_i and t_j are obtained from their respective input representations passed through their respective neural network branch. The two resulting embeddings are aggregated to a single score by their (scaled) dot product. The cross-entropy loss optimizes this score to be maximal or minimal for positive or negative combinations of microbial spectra and drugs, respectively.

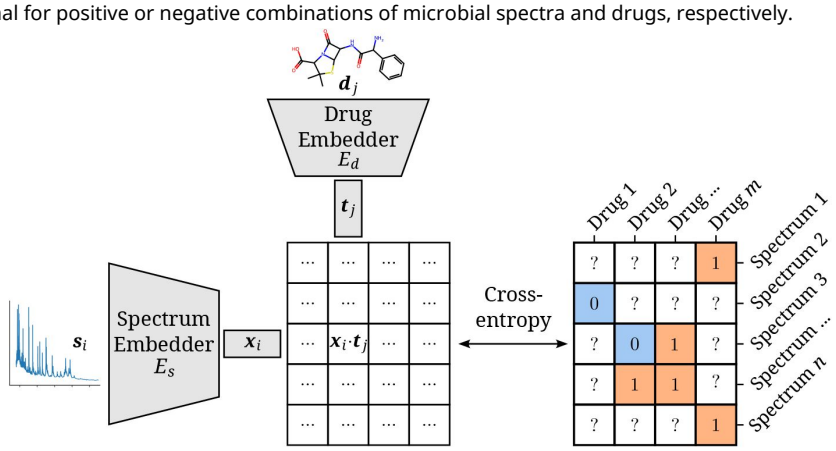

Table 1.

All tested model sizes for the (instance) spectrum branch. Hidden sizes represent the evolution of the hidden state dimensionality as it goes through the model, with every hyphen defining one fully connected layer. The listed number of parameters only include those of the instance (spectrum) branch.

Size	# Weights	Hidden sizes
S	1 578 176	6000-256-128-64
M	3 246 784	6000-512-256-128-64
L	6 846 144	6000-1024-512-256-128-64
XL	15 093 440	6000-2048-1024-512-256-128-64

3. As DeepSMILES strings (O'Boyle and Dalke, 2018) paired with a 1D convolutional neural network (CNN).
4. As DeepSMILES strings paired with a gated recurrent unit neural network (GRU).
5. As DeepSMILES strings paired with a transformer neural network.
6. As images paired with a 2D CNN.
7. As rows of a pre-computed string kernel on the SMILES strings (LINGO (Vidal et al., 2005)), paired with a single linear layer.

For all these combinations, the embedder outputs target embeddings $t_j \in \mathbb{R}^{64}$. For more details on the different drug embedders and their hyperparameters (as well as their tuning), see Appendix B. For every combination of spectrum embedder (four sizes: S, M, L, and XL) and drug embedder (seven types), six different learning rates ({ 1e-5, 5e-5, 1e-4, 5e-4, 1e-3, 5e-3 }) are tested. For all these different combinations, five models are trained (using different random seeds for model initialization and batching of data). For every spectrum and drug embedder combination, only results from the best learning rate are presented; that is, the learning rate resulting in the best average validation ROC-AUC for that combination.

All models are trained with the Adam optimizer (Kingma and Ba, 2014) for a maximum of 50 epochs with a batch size of 128. A linear learning rate warmup over the first 250 steps is applied, after which the rate is kept constant. As every epoch constitutes one pass over every label and, hence, multiple passes over every individual drug and spectrum, a branch can technically already be overfitting before the end of the first epoch. Because of this, performance on the validation set is checked every tenth of an epoch. Training is halted early when validation ROC-AUC hasn't improved for 10 validation set checks. The checkpoint of the best performing model (in terms of validation ROC-AUC) is used as the final model.

4. Results

The following section will first relay the results of the different dual-branch model configurations. After, the "general" AMR recommender is matched up against "species-specific" and "species-drug-specific" models. Finally, the models' capabilities and representations are examined through transfer learning and embeddings.

4.1 Encoding species and drugs effectively

Figure 2 shows the performance of all trained models in terms of their average ROC-AUC and Prec@1(-). It can be seen that, in general, performance differences between model configurations occupy a small margin. However, trends can still be found. Models using Morgan Fingerprints typically outperform other drug embedding strategies. Morgan Fingerprints provide a compressed and pre-processed input format, the nature of which provides an apparent advantage over input representations that require more pattern extraction. The small number of different antimicrobial drugs may not be conducive to learning complex representations. Indeed, embedding drugs without a compound information (i.e. one-hot embedding) is a competitive approach for this problem, resulting in the on average second best models in terms of ROCAUC. On the spectrum embedder side, it is observed that the medium or large variants typically perform best. The full ROC curve (showing sensitivity and specificity) for the best-performing model is shown in **Figure 8**.

Performance in terms of Macro ROC-AUC can be found in **Figure 9**. The Macro ROC-AUC averages the ROC-AUC for every individual drug. Here, Morgan fingerprints similarly reach the best performances. The full list of performances can be found in **Table 5**.

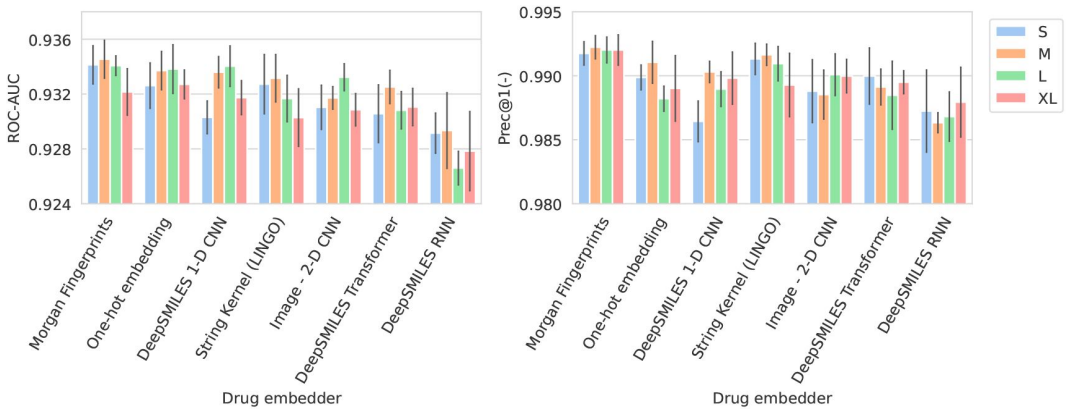

Figure 2.

Barplots showing test performance results for all trained models. ROC-AUC evaluates overall ranking of predictions. Prec@1(-) evaluates how often the top suggested treatment would be effective. Both metrics are calculated per spectrum/patient and then averaged. Errorbars represent the standard deviation over five random model seeds. The x-axis and colors show the different drug and spectrum embedders, respectively.

In **Figure 10**, the performance of the spectrum embedder sizes is compared against a linear baseline. The linear baseline uses the same preprocessed input spectrum representation, but only uses a single linear combination to produce an embedding. For this comparison, only the Morgan fingerprint drug embedders are used, as they produce the best-performing models overall. Models using nonlinear multi-layer spectrum embedders obtain considerably better performance over linear embedders.

4.2 Species-specific models improve recommendation

The recommender systems presented in §4.1 provide an incredibly general tool. Trained as single models for all species and drugs, their versatility is unparalleled compared to previous studies that create classifiers for specific drug-species combinations (Weis et al., 2020b). In between the extremes of "one model for everything" and "a model per species and per drug", there lies a compromising approach: a speciesspecific recommender system for all drugs. Such recommender systems would be more specialized in nature, but their usefulness hinges upon having done prior species identification. As these are typically included in the MS' manufacturers software, a more specialized species-specific recommender may provide better performance without incurring extra cost. The disadvantage of such models is that (1) they can not be used for species for which there is not enough data to train a separate model (i.e. rarely occurring species), and (2) they rely on the prior identification step to be correct.

Here, we create species-specific recommender models for the 25 most-occurring species in DRIAMS-A. The training setup for these models is kept the same as in §4.1. The difference between "general" recommenders and "species-specific recommenders" is that each species-specific recommender model is only trained on the subset of data covering their respective species (As these models use a smaller training set, validation is checked every fourth of an epoch instead of every tenth). Together, the test predictions of the 25 species-specific recommenders cover 4229 spectra, 56 drugs, and 69827 AMR labels (covering 91.27% of the original test set). **Table 2** compares the two best "general" recommenders from §4.1 to their species-specific recommender counterparts. It is observed that species-specific recommenders deliver better predictions across all evaluated metrics.

As opposed to the species-specific models, the "general" recommender can use learned representations from one species to enhance predictions for other species, benefitting from multi-task learning. The fact that this latter mode of learning performs worse on this problem, however, indicates that such transfer of learned knowledge is of limited usefulness for AMR prediction. Still, the "general" recommender model remains useful in instances where the species could not be identified, or is rare. In **Table 6**, the 25 species for which specific recommenders were trained are listed, along with their performances.

4.3 Dual-branch recommenders improve over baselines

In order to gain better insight into the performance of our models, in this section, both our "general" and "species-specific" recommenders are squared up against extensive baselines.

Previous studies have studied AMR prediction in specific species-drug combinations. For this reason, it is useful to compare how the dual-branch setup weighs up against training separate models for separate species and drugs. In Weis et al. (2020b), for example, binary AMR classifiers are trained for the following three combinations: (1) *E. coli* with Ceftriaxone, (2) *K. pneumoniae* with Ceftriaxone, and (3) *S. aureus* with Oxacillin. Here, such "species-drug-specific classifiers" are trained for the 200 most-common combinations of species and drugs in the training dataset. For these combinations, binary logistic regression, XGBoost (Chen and Guestrin, 2016) and MLPs are tested. The tested MLPs come in the same four sizes as the spectrum branches of the

Model	ROC-AUC	Prec@1(-)	Macro ROC-AUC
General Recommender (Morgan Fingerprints - M)	0.9411 ± 0.0007	0.9967 ± 0.0011	0.7684 ± 0.0050
General Recommender (One-hot - L)	0.9408 ± 0.0011	0.9940 ± 0.0009	0.7746 ± 0.0316
Species-spec. Recommenders (Morgan Fingerprints - M)	0.9461 ± 0.0010	**0.9973 ± 0.0004**	**0.7905 ± 0.0151**
Species-spec. Recommenders (One-hot - L)	**0.9468 ± 0.0012**	0.9950 ± 0.0011	0.7686 ± 0.0155

Table 2.

Test performance of selected general and species-specific dual branch recommender models. The listed averages and standard deviations are calculated over five independent runs of the same model. Performance is computed on the subset of labels spanning the 25 most-common species in DRIAMS-A.

dual-branch models. Other than having an output node of size 1 for binary classification, they share all hyperparameters with the tested spectrum branches. For details on the training and tuning procedure of all baselines, see Appendix B.2.2.

There exist many species-drug combinations for which there are either only positive or only negative labels. As it is impossible to train and evaluate models for these cases, models are trained only for the 200 most-occurring combinations for which both labels are present in the training, validation and test set. We refer to these models as "species-drug classifiers".

In addition, it is useful to probe model performance against what experts may be able to guess. Given knowledge of the species identity in question, an expert will in many cases already be able to make a good guess towards what drugs will be effective or not. Hence, baseline "best guess" performance would not result in a ROC-AUC of 0.5. A way to simulate such "expert's best guess" baseline predictions is through counting label frequencies in the training set. More specifically, for a test label belonging to a certain species and drug, the labels in the training set corresponding to that drug and species can be gathered. The frequency by which that training set is positive or negative can be used to infer a test predicted probability. We refer to this baseline as "simulated expert's best guess".

Table 3 compares the recommenders from §4.2 to non-recommender baselines. As the baselines are only trained on the 200 most-common species-drug combinations, performance is computed on that subset of test labels. This reduced test set spans 4017 spectra, 35 drugs, and 53503 labels (covering 70.28% of the original test set). Dual-branch recommenders outperform baselines on all but one metric. Logistic regression baselines result in the best average ROCAUC for individual species-drug combinations. By all other metrics, dual-branch recommenders outshine a collection of species-drug-specific classifiers. It's illustrated that, when the question is to choose between drugs for a patient (evaluated by the patient-averaged ROC-AUC or Prec@1(-)), a model designed as a recommender will outperform binary classification models trained to predict AMR for specific drugs. On the other hand, species-specific binary classifiers are optimal for distinguishing spectra for a specific drug. The crux of our case in favor of recommender models relies, hence, on the fact that patient-averaged metrics are more representative of AMR models' utility in clinical diagnostics.

It is useful to note that *any* gain in performance over the "simulated expert" means that AMR signal could be mined from the spectra. Hence, any performance above this level results in a real-world information gain for clinical diagnostic laboratories.

4.4 Efficient transfer learning to new hospitals

An AMR prediction model trained using data from one hospital may not be suitable for use in other hospitals for several reasons. First, protocols such as sample preparation and culturing media differ from hospital to hospital, resulting in systematic differences in MALDI-TOF spectra (Weis et al., 2022). Second, epidemiology is spatially varied. Drug-resistant clades may be prevalent in one region or country, but absent in another (Humphries, 2022). Finally, the MALDITOF instruments themselves may also be specific to the hospital and influence the readout. This influences prediction models, as a hospital-specific effect is reported by the study introducing the DRIAMS dataset (Weis et al., 2022). They find that models typically perform best when trained with data from the same hospital. Here, hospital transferability is studied in the context of transfer learning.

Data from DRIAMS-B, -C and -D, are split into training, validation and test set. The train set for these hospitals consists of 1000 randomly-drawn spectra, simulating a small data scenario where the hospital has not spent considerable efforts in data collection. The remaining spectra for all three hospitals are evenly split among validation and test set.

Model	ROC-AUC	Prec@1(-)	Macro ROC-AUC	Species-drug Macro ROC-AUC
Species-spec. Recommenders (Morgan Fingerprints - M)	0.9009 ± 0.0018	**0.9830 ± 0.0015**	**0.8283 ± 0.0059**	0.6381 ± 0.0121
Species-spec. Recommenders (One-hot - L)	**0.9030 ± 0.0018**	0.9814 ± 0.0020	0.8129 ± 0.0079	0.6511 ± 0.0290
General Recommender (Morgan Fingerprints - M)	0.8939 ± 0.0016	0.9746 ± 0.0006	0.8114 ± 0.0064	0.6517 ± 0.0076
General Recommender (One-hot - L)	0.8933 ± 0.0020	0.9778 ± 0.0023	0.8124 ± 0.0033	0.6521 ± 0.0078
Species-drug classifiers (MLP - S)	0.8341 ± 0.0135	0.9420 ± 0.0123	0.8005 ± 0.0032	0.6745 ± 0.0218
Species-drug classifiers (MLP - M)	0.8382 ± 0.0077	0.9421 ± 0.0196	0.8075 ± 0.0049	0.6797 ± 0.0097
Species-drug classifiers (MLP - L)	0.8457 ± 0.0088	0.9505 ± 0.0100	0.8037 ± 0.0079	0.6648 ± 0.0149
Species-drug classifiers (MLP - XL)	0.8611 ± 0.0049	0.9722 ± 0.0041	0.8106 ± 0.0069	0.6801 ± 0.0101
Species-drug classifiers (Logistic Regression)	0.8684	0.9432	0.7989	**0.7200**
Species-drug classifiers (XGBoost)	0.8346	0.9196	0.7763	0.6236
Simulated expert's best guess	0.8681	0.9743	0.7159	0.5000

Table 3.

Test performance of selected recommender models, compared to the performance of a collection of models — each trained on only one species-drug combination — coined "species-drug classifiers". "Speciesdrug classifiers" refer to a collection of binary classifiers, each trained to predict AMR status for a subset of data comprising a single species-drug combination. "Simulated expert's best guess" refers to counting AMR label frequencies in single species-drug combinations, and taking those as predictions. The listed averages and standard deviations are calculated over five independent runs of the same model. Given the non-stochastic nature of the logistic regression and XGBoost implementations, only one set of models is trained and, hence, no standard deviations are reported. Performance is computed on the subset of labels spanning the 200 mostcommon species-drug combinations.

For all three hospitals, we train models in the same way as previously (see §3.3). A comparison is made between fine-tuning starting from models trained on DRIAMS-A (i.e. models from previous sections) and dual-branch models trained from scratch (**Figure 3**). For simplicity, we transfer the non-species-specific, "general" recommenders, as we feel this reflects a more realistic use-case for labs that cannot afford to gather spectra for all possible species and additionally fine-tune them. Over all three hospitals, models finetuned from a DRIAMS-A checkpoint generally outperform models trained from scratch. This trend holds true over different numbers of spectra available in the fine-tuning set. In general, it can be seen that pretrained models require very little fine-tuning spectra to obtain performances in the same order of magnitude as with DRIAMS-A (§4.1). Performance comparisons of the same models in terms of other metrics are shown in **Figure 11**

Lowering the amount of data required is paramount to expedite the uptake of AMR models in clinical diagnostics. The transfer learning qualities of dual-branch models may be ascribed to multiple properties. First of all, since different hospitals use much of the same drugs, transferred drug embedders allow for expressively representing drugs out of the box. Secondly, owing to multi-task learning, even with a limited number of spectra, a considerable fine-tuning dataset may be obtained, as all available data is "thrown on one pile".

4.5 MALDI-TOF spectra embeddings

To investigate what the dual-branch models have learned to represent, MALDI-TOF spectra embeddings are examined. For this purpose, both the bestperforming "general" recommender and "speciesspecific" recommender are used. Here, we visualize the embeddings $x_i \in \mathbb{R}^{64}$ of all test set spectra from the 25 most-occurring pathogens. To visualize in a 2dimensional space, UMAP is applied (using default parameters apart from min_dist=0.5; increasing this parameter helps reduce UMAP packing points too tightly together, hence, making for a more-legible plot). **Figure 4** shows the resulting embeddings, colored by species identity, as well as by their AMR status to a selection of drugs.

The MALDI-TOF embeddings from the "general" recommender model are grouped primarily per species. This shows that, without being instructed to discriminate between species, the model has learned to group spectra of the same species together. Furthermore, species under the same genus are typically grouped close together, illustrating that the model can pick up hierarchical relations in the tree of life from the data. Within species clusters, the AMR status subplots show that samples are often grouped according to their resistance. For example, for *S. epidermidis* and *S. aureus*, multidrug resistant variants clearly form subclusters. In addition, the cluster of *E. coli* spectra shows a clear tail with samples resistant to ciprofloxacin. Embeddings from the species-specific recommender models show this phenomenom more clearly. UMAP embedding plots from the "general recommender" colored by other drugs are shown in **Figure 12**. In addition, species-specific recommender system embeddings for some prominent species are shown in **Figure 13**.

5. Discussion

Prior work on AMR prediction has always modeled within the boundaries of one clade and drug(class), using standard machine learning practices. This work differentiates itself from others by constructing one model for the whole range of drugs encountered in clinical diagnostics. We propose to model AMR prediction via dual-branch neural networks, producing a novel MALDI-TOF-based AMR recommender system. The proposed models come with improved performance over the approaches taken in previous works.

Figure 3.

Transfer learning of DRIAMS-A models to other hospitals. Errorbands show the standard deviation over five runs. Results in terms of other evaluation metrics are shown in **Figure 11**.

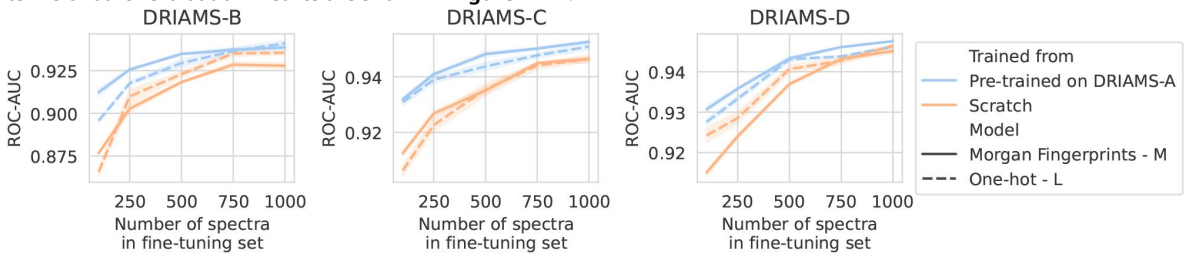

Figure 4.

UMAP scatterplots of test set MALDI-TOF spectra embeddings x_i. **Top:** Embeddings from a "general" (trained on all species) recommender. Only embeddings belonging to the 25 most-occurring species in the test set are shown. The panels on the right show the same embeddings as on the left, but colored according to its AMR status to a certain drug. The four displayed drugs are selected based on a ranking of the product of the number of positive and negative labels $\sum_{i=1}^{n}[y_{ij} = 0] \cdot \sum_{i=1}^{n}[y_{ij} = 1]$. In this way, the drugs that have a lot of observed labels, both positives and negatives, are displayed. **Bottom:** Highlighted embeddings from a *S. epidermidis* specific recommender model.

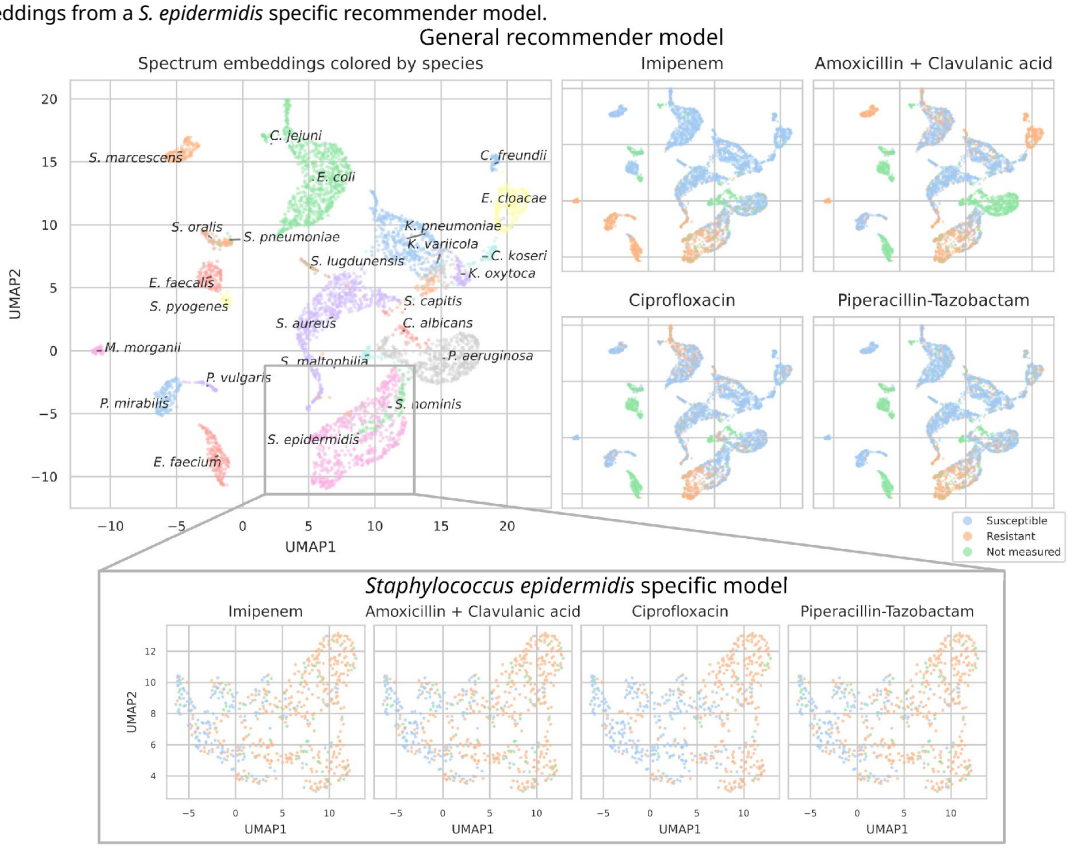

In clinical diagnostics, AMR predictions could be used to decide which drug to administer on a perpatient basis. For this reason, we argue that evaluation metrics should probe the average quality of predictions per patient (i.e. spectrum-macro metrics). We show that, for these metrics, recommender systems consistently outperform baselines.

We postulate that the performance of the proposed models is still limited due to (1) lacking a MALDI-TOFspecific learning architecture, (2) collection of more data, especially on rarely-encountered species and drugs, and (3) inherent technological limitations of MALDI-TOF MS. Whilst the former is the subject of further machine learning research, the latter two can be considered by equipping the model with some notion of uncertainty, epistemic and aleatoric, respectively (Hüllermeier and Waegeman, 2021). In medical decision-making applications, effective uncertainty estimates would be an invaluable tool to aid understanding the models' predictions. A fourth factor to consider is that perfect test set performance may also be unattainable due to labeling errors. This comes as a consequence of (1) error-prone laboratory measurements of MIC values, and (2) the fact that EUCAST norms change over time, resulting in outdated label thresholds for historical data.

As bacterial strains readily adapt resistance to new and frequently-used antibiotics, it is impossible for an AMR model to maintain its performance over time. Consequently, an obvious need for continual data collection and online machine learning approaches presents itself. It is for this reason that ML for AMR prediction will prove most valuable when integrated tightly in the inner workings of healthcare (Lee and Lee, 2020).

It stands to reason that blindly following the recommender system's predictions spells misery. For example, healthcare practitioners should additionally take into account host-specific factors such as patient age, medical history, and concurrent medication. Additionally, as the model is trained on the whole repertoire of antimicrobial drugs, it will have learnt that broad-spectrum antibiotics are typically effective. Hence, it may overrecommend their use. As a consequence, the model's proposed treatment strategies may not be aligned with antibiotic stewardship, instead exacerbating the very issue it is designed to mitigate. To tackle this problem, one could downweigh the prediction probabilities of undesirable drugs, or, alternatively, train a dual-branch model on only more-specifically-working drugs.

In summary, this study serves as the first proofof-concept for large MALDI-TOF-based antimicrobial drug recommenders. In this context, we highlight the need for appropriate metrics, proposing that perpatient metrics are most suitable. Extensive experiments on our proposed dual-branch model allow us to assemble some conclusions w.r.t. its use. Firstly, we find that medium-sized MLP spectrum embedders (counting 3.2M weights) generally perform best. Second, incorporating chemical information works best using Morgan Fingerprints. Third, while more data may skew the favor towards the other side, given the current available data, species-specific models outperform recommenders trained for all species. For the smaller datasets used in the transfer learning experiments, the structural inductive bias lent to the model via Morgan fingerprints delivers best results. Our experiments demonstrate that dual-branch recommenders outperform non-recommender baselines on relevant metrics. In the above discussion, some considerations are listed w.r.t. its practical implementation in healthcare. Taken together, this work demonstrates the potential of AMR recommenders to greatly extend the value of MALDI-TOF MS for clinical diagnostics.

Acknowledgements

This work was supported by Research Foundation Flanders (FWO) [PhD Fellowship fundamental research grant 1153024N to G.D.W.]. W.W. also received funding from the Flemish Government under the "Onderzoeksprogramma Artificiële Intelligentie (AI) Vlaanderen" Programme

A. DRIAMS processing

As our models require every target to correspond to one specific drug (for which a SMILES string can be obtained), data provided by Weis et al. (2022) is further cleaned up. First, as "Quinolones", and "Aminoglycosides" constitute classes of drugs rather than single ones, these drugs and their corresponding measurements are removed from the dataset. Second, some drug names in DRIAMS that refer to the same chemical structure are merged to a single drug. As this merging of drugs also combines their labels, care is taken so that no conflicting labels are combined. If, for a single spectrum, labels exist for both of the merging drugs in question, the label is only kept if both measurements are congruent (either both resistant, intermediate or susceptible). Otherwise, the merged label is discarded. Finally, some drugs are renamed such that there is less ambiguity as to exactly which compound is referred to by their name. The full list of modifications to drug names is listed in **Table 4**.

To present drugs to the model, all names of drugs are converted to SMILES strings. In this work, PubChem's canonical SMILES strings of every compound are used. In PubChem, canonical SMILES are not isomeric, which means that stereochemistry is ignored. As such, two drugs that are stereoisomers are treated as a single drug, this is the case for Ofloxacin and Levofloxacin. Furthermore, many drugs in the dataset refer to the co-administration of two compounds (such as, for example, Ampicillin-Sulbactam or AmoxicillinClavulanic acid). These cases are treated as a single drug with a SMILES string consisting of the strings of both constituent compounds separated by a "." character, as is common practice with SMILES strings.

B. Modeling set-up

B.1. Drug embedders

In this paper, seven ways to encode drugs in a model are tested out. In this section, those seven drug embedders are described in detail. All descriptions correspond to the final set-up used to present results, hyperparameter tuning results are presented in **Appendix B.2.1**.

All drug embedders encode drugs to a vector $t_j \in \mathbb{R}^{64}$. The most simple way to obtain a dense vector of that size for every drug is via a **one-hot embedding**. Every drug gets assigned an index in a vector, and the resulting vectors are embedded to a dense representation via a single linear layer. Encoding drugs in this way is the most straightforward, but no structural information of the underlying active compound is included. No inductive bias is presented to the model that will give structurally-similar drugs comparable embeddings. As such, all this information must be learnt from data. Similarly, such drug embedders can not be generalized out-of-the-box to drugs it hasn't seen in the training data, as there are no indicesand learnt embeddings - for them.

The (local) structure of drugs can be encoded via fingerprints. A molecular fingerprint corresponds to a bit-vector in which every bit corresponds to the presence or absence of a substructure (Capecchi et al., 2020). In this paper, **Morgan fingerprints** with a diameter of 4 and consisting of 512 bits are derived from RDKit (Landrum, 2013). The resulting vector is embedded with a linear layer to get a dense drug representation. Embedding drugs using such structural features overcomes the aforementioned drawbacks with one-hot embeddings.

Similarly, the identity of a drug can be communicated via the textual representation known as SMILES strings (Weininger, 1988). Here, an adaptation of SMILES for machine and deep learning applications is used, called DeepSMILES (O'Boyle and Dalke, 2018). All the different letters in the

Original drug name	Step undertaken
Quinolones	Removed
Aminoglycosides	Removed
Ofloxacin	Merged with Levofloxacin
Benzylpenicillin	Merged with Penicillin
Benzylpenicillin_others	Merged with Penicillin
Benzylpenicillin_with_meningitis	Merged with Penicillin
Benzylpenicillin_with_pneumonia	Merged with Penicillin
Penicillin_with_endokarditis	Merged with Penicillin
Penicillin_without_endokarditis	Merged with Penicillin
Penicillin_without_meningitis	Merged with Penicillin
Penicillin_with_meningitis	Merged with Penicillin
Penicillin_with_pneumonia	Merged with Penicillin
Penicillin_with_other_infections	Merged with Penicillin
Cefuroxime.1	Merged with Cefuroxime
Cotrimoxazol	Merged with Cotrimoxazole
Gentamicin_high_level	Merged with Gentamicin
Cefoxitin_screen	Merged with Cefoxitin
Teicoplanin_GRD	Merged with Teicoplanin
Vancomycin_GRD	Merged with Vancomycin
Rifampicin_1mg-l	Merged with Rifampicin
Meropenem_with_meningitis	Merged with Meropenem
Meropenem_without_meningitis	Merged with Meropenem
Meropenem_with_pneumonia	Merged with Meropenem
Amoxicillin-Clavulanic acid_uncomplicated_HWI	Merged with Amoxicillin-Clavulanic acid
Strepomycin_high_level	Renamed to Streptomycin
Bacitracin	Renamed to Bacitracin A
Ceftarolin	Renamed to Ceftaroline fosamil
Fosfomycin-Trometamol	Renamed to Fosfomycin Tromethamine

Table 4.

Full list of modifications made to drug names in DRIAMS. Modifications consist of (1) removal of drugs, (2) merging of drugs, and (3) renaming drugs.

Drug embedder	Spectrum embedder	ROC-AUC	Prec@1(-)	Macro ROC-AUC
Morgan Fingerprints	S	0.9341 ± 0.0014	0.9917 ± 0.0009	**0.8158 ± 0.0070**
	M	**0.9345 ± 0.0014**	**0.9922 ± 0.0009**	0.8078 ± 0.0081
	L	0.9341 ± 0.0007	0.9920 ± 0.0010	0.8070 ± 0.0128
	XL	0.9322 ± 0.0017	0.9920 ± 0.0012	0.7904 ± 0.0155
One-hot embedding	S	0.9326 ± 0.0017	0.9899 ± 0.0010	0.7984 ± 0.0086
	M	0.9337 ± 0.0014	0.9910 ± 0.0016	0.7920 ± 0.0175
	L	0.9338 ± 0.0018	0.9882 ± 0.0010	0.8011 ± 0.0116
	XL	0.9327 ± 0.0011	0.9890 ± 0.0026	0.7932 ± 0.0201
DeepSMILES 1-D CNN	S	0.9303 ± 0.0012	0.9864 ± 0.0016	0.7949 ± 0.0185
	M	0.9336 ± 0.0011	0.9903 ± 0.0008	0.8009 ± 0.0044
	L	0.9337 ± 0.0015	0.9890 ± 0.0014	0.7940 ± 0.0052
	XL	0.9317 ± 0.0012	0.9898 ± 0.0020	0.7960 ± 0.0155
String Kernel (LINGO)	S	0.9327 ± 0.0022	0.9913 ± 0.0012	0.7972 ± 0.0087
	M	0.9332 ± 0.0017	0.9916 ± 0.0008	0.7919 ± 0.0051
	L	0.9317 ± 0.0017	0.9909 ± 0.0013	0.7859 ± 0.0136
	XL	0.9303 ± 0.0021	0.9893 ± 0.0025	0.7935 ± 0.0135
Image - 2-D CNN	S	0.9310 ± 0.0016	0.9888 ± 0.0025	0.7820 ± 0.0101
	M	0.9317 ± 0.0008	0.9885 ± 0.0019	0.7866 ± 0.0084
	L	0.9332 ± 0.0010	0.9901 ± 0.0016	0.7758 ± 0.0070
	XL	0.9309 ± 0.0012	0.9900 ± 0.0013	0.7711 ± 0.0109
DeepSMILES Transformer	S	0.9306 ± 0.0021	0.9900 ± 0.0022	0.7862 ± 0.0124
	M	0.9325 ± 0.0012	0.9891 ± 0.0014	0.7925 ± 0.0075
	L	0.9308 ± 0.0014	0.9885 ± 0.0027	0.7902 ± 0.0072
	XL	0.9311 ± 0.0014	0.9895 ± 0.0009	0.7791 ± 0.0075
DeepSMILES RNN	S	0.9291 ± 0.0015	0.9872 ± 0.0032	0.7881 ± 0.0053
	M	0.9293 ± 0.0028	0.9863 ± 0.0008	0.7793 ± 0.0116
	L	0.9266 ± 0.0012	0.9868 ± 0.0019	0.7684 ± 0.0058
	XL	0.9278 ± 0.0029	0.9879 ± 0.0027	0.7689 ± 0.0113

Table 5.

Full table of test results. The listed averages and standard deviations are calculated over five independent runs of the same model. The best models for every metric per drug embedder are underlined. The overall best model for every metric is in bold face.

Species	ROC-AUC
Staphylococcus aureus	0.9578
Staphylococcus epidermidis	0.9478
Escherichia coli	0.9184
Klebsiella pneumoniae	0.9643
Pseudomonas aeruginosa	0.7614
Enterobacter cloacae	0.9831
Proteus mirabilis	0.9727
Staphylococcus hominis	0.9594
Serratia marcescens	0.9848
Staphylococcus capitis	0.9425
Enterococcus faecium	0.9914
Klebsiella oxytoca	0.9861
Klebsiella variicola	0.9824
Citrobacter koseri	0.9970
Enterococcus faecalis	0.9594
Staphylococcus lugdunensis	0.9705
Citrobacter freundii	0.9622
Morganella morganii	0.9931
Proteus vulgaris	0.9828
Staphylococcus haemolyticus	0.9751
Candida albicans	0.7446
Streptococcus pneumoniae	0.9059
Stenotrophomonas maltophilia	1.0000
Campylobacter jejuni	1.0000
Haemophilus influenzae	1.0000

Table 6.

Test ROC-AUC performance per species. Reported figures are averages across the five different Medium-sized Morgan Fingerprint-based recommenders.

alphabet are assigned an index in a one-hot vector. Hence, every molecule can be encoded to a matrix $s_j \in \mathbb{R}^{v \times l}$, with v the vocabulary size of the DeepSMILES alphabet and l the string length of the molecule. This representation can be processed to a vector embedding using any neural network type that is appropriate for variable-length sequences.

A **1D CNN** detects and composes local patterns in the DeepSMILES string to a final drug embedding. Every input channel corresponds to a specific letter in the SMILES alphabet. The convolutional network used here consists of a position-wise linear layer to embed the channels to 64 dimensions, four convolutional blocks placed in sequence, followed by a global max-pooling operation across the length axis and a final linear layer to return a vector $t_j \in \mathbb{R}^{64}$. The global max-pooling layer allows the same network to be used for variable-length inputs. Each convolutional block consists of a structure similar to the one found in transformers (Vaswani et al., 2017). A first layer normalization is followed by a (padded) convolutional layer with a kernel size of 5, a first residual connection is wrapped around these two operations. After this, a position-wise feedforward makes up the second half of the convolutional block. The positionwise feedforward consists of a layer normalization, after which a GeLU-based gated linear unit identical to the one introduced by Shazeer (2020) is employed: $z = Dropout_{0.2}((GeLU(xW) \odot xV))W_2$. First, the input is sent to two position-wise linear layers via W and V, each of them exploding the hidden dimensions of the input by a factor of four. By sending the result of the first linear layer to a GeLU activation and multiplying element-wise with the result of the second linear layer, a gated linear unit structure is obtained. The output of this gated linear unit is sent to a dropout layer with rate 0.2 and then returned to the original dimension size via a final linear layer W_2. Around this second LayerNorm and feedforward structure, a residual connection is again wrapped. All residual blocks have an input and output hidden dimension of 64. **Figure 5** shows the structure of this convolutional block. Its design adopts the current state-of-the-art practices in transformers, which are increasingly being used in convolutional networks (Liu et al., 2022).

A **transformer** can be used to learn and compose signals in the DeepSMILES strings that occur sequence-wide, as opposed to the local pattern detection with a 1D CNN. The DeepSMILES strings are similarly embedded to 64 dimensions per character. After this, sinusoidal positional encodings (Vaswani et al., 2017) are added, and a CLS token embedding is prepended to the sequence. Four transformer blocks are employed, each with 64 as hidden dimen-sion. The structure of the blocks are identical as with the 1D CNN (**Figure 5**), but using scaled dot-product self-attention instead of 1D convolutions. The selfattention operation uses 8 heads. The output at the CLS token is used as a "summary" of the content in the sequence (as opposed to the global max pooling with the CNN). A final linear layer on the output of the CLS token returns the drug embedding $t_j \in \mathbb{R}^{64}$.

A **recurrent neural network** (RNN) is used to process the DeepSMILES strings sequentially. The RNN used here consists of a bidirectional GRU with 64 hidden dimensions (Cho et al., 2014). The two final hidden states of the GRU are used as "summaries" of the content in the sequence. These two final states are averaged (element-wise) and sent to a final linear layer returning $t_j \in \mathbb{R}^{64}$.

All three aforementioned neural network structures work on variable-length (Deep)SMILES strings. With mini-batches, input drugs are (zero) padded so that everything fits into a tensor $S \in \mathbb{R}^{b \times v \times l}$, with b the batch size, v the vocabulary size, and l the longest length of a drug in the batch. The three aforementioned neural nets are adapted so that no information can flow from masked tokens to actual drug tokens (through masking after convolutions or in the attention matrices).

As (Deep)SMILES are a 1D representation of a 3D molecular structure, a more-detailed view of the drug may be obtained by permitting an extra dimension into its input representation. Drawings of drugs achieve this 2D view of the molecule. Here, 128 × 128 drawings of drugs are obtained through RDKit. The RGB values are inverted so as to make the parts of the image containing molecule "activated". Also, the RGB values are scaled to the range of 0 to 1 by dividing by 255. A **2D CNN** processes the images to a drug embedding. The CNN consists of an input convolutional layer

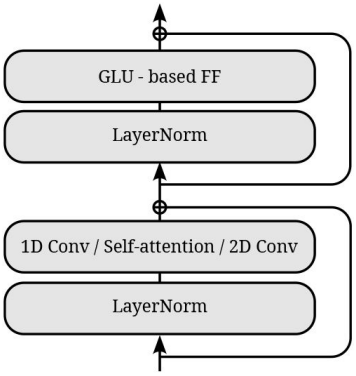

Figure 5.

Structure used for the residual blocks, used in the 1D CNN, 2D CNN, and transformer. In the case of convolutions, the output is zero padded so as to produce the same output dimensions as in the input.

with kernel size and stride of 2. The input layer takes the three input channels and returns 32 hidden dimensions. After, two convolutional blocks of the same structure as with the transformer and 1D CNN are placed in tandem (**Figure 5**). The 2D convolutional operation used in the convolutional operation has a kernel size of 5. Hereafter, a global max-pooling operation across the height and width of the image is performed, followed by a final linear layer producing the drug embedding $t_j \in \mathbb{R}^{64}$.

A final way to obtain a numerical representation of drugs tested here is through similarity matrices. A **string kernel** is used to create a Gram matrix of all drugs in the training set. The input representation of a drug is then simply a row in said Gram matrix. This approach is generalizable to unseen drugs at inference time, as obtaining a representation for them involves running the kernel function of the new compound to all training drugs. In this work, the LINGO string kernel (using 4-mers) is used (Vidal et al., 2005), as this kernel performed well in a recent benchmark (Öztürk et al., 2016). Note that here, SMILES strings are used instead of DeepSMILES (as with the 1D CNN, RNN, and transformer). A linear layer produces the fi-nal drug embedding $t_j \in \mathbb{R}^{64}$ from a row in the Gram matrix.

A visual overview of all seven drug embedders in given in **Figure 6**.

B.2. Hyperparameter tuning

B.2.1. Dual-branch models

Due to the complexity of tuning two branches and the size of the dataset, tuning is mostly done in an *ad hoc* fashion, relying on knowledge of current best practices in deep learning. Only some hyperparameters of interest are tuned on the validation set. Here, we present validation model results of those experiments. All results presented here concern models that are trained with a medium-sized spectrum embedder, with hyperparameters otherwise as described in Appendix B.1. All numbers indicate an average over five runs, similarly choosing the best average out of four tested learning rates (1e-5, 5e-5, 1e-4, 5e-4, 1e-3, 5e-3).

Figure 7A shows validation set performances for a grid of different kernel sizes and hidden dimensionalities for the SMILES 1-D CNN. The bestperforming hidden dimensionality (64) is copied to the (Deep)SMILES Transformer and GRU without further tuning. In **Figure 7B**, a similar grid is shown for the Image 2-D CNN, where it is found that a smaller hidden size is favored. **Figure 7C** shows the performance for using different molecular string representations as input to the 1-D CNN model: SMILES, DeepSMILES (O'Boyle and Dalke, 2018), and SELFIES (Krenn et al., 2020). While all techniques perform competitively, DeepSMILES strings outperform the other two by a small margin. Similarly, DeepSMILES are thus selected as input representations for the Transformer and GRU, without further tuning. **Figure 7D** shows how sinusoidal positional encodings outperform learned positional encodings (as in Devlin et al. (2018)). It is found that a bidirectional GRU considerably outpeforms a unidirectional one (**Figure 7E**). Finally, the number of bits in the Morgan fingerprint encoding is also tuned (**Figure 7F**). It is seen that including lower than 512 bits degenerates performance, but including more than 512 introduces instabilities in model training, as the model becomes prone to overfitting the drug branch.

B.2.2. Specialist baselines

All baselines are trained using the same data splits as used with the dual-branch model. In essence: all DRIAMS-A spectra before the year 2018 are in the training set. The remaining spectra from 2018 are evenly divided among validation and test (with which belonging to which

Figure 6.

Overview of all different drug embedders tested in this work. One-hot embeddings are the only technique not incorporating prior knowledge of the structure of the compound. Hence, they are the only technique incapable of directly transferring to new compounds. Morgan fingerprints produce a bit-vector containing information on the presence of certain substructures. DeepSMILES strings are encoded and processed with a 1D CNN, GRU, or transformer. Drawings of molecules are processed with a 2D CNN. A string kernel on SMILES strings produces a numerical vector for every drug (taken as the row in the resulting Gram matrix).

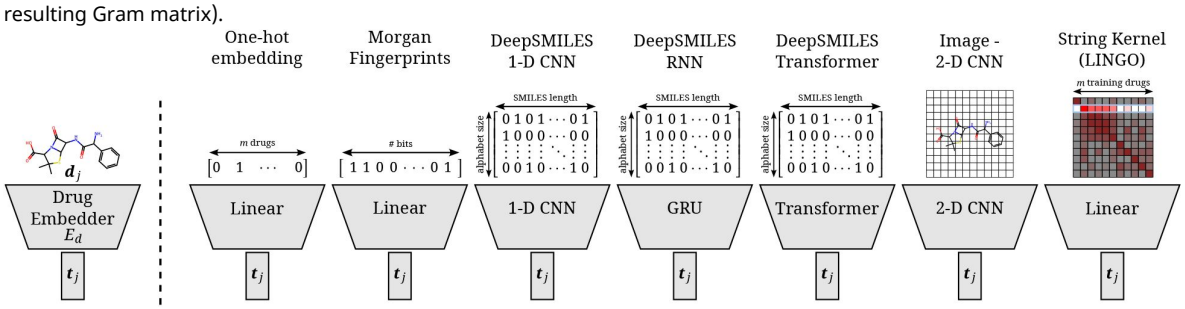

Figure 7.

All hyperparameter tuning experiments. All evaluations are listed in terms of validation ROCAUCs. All numbers are averages of five model runs, with errorbars showing standard deviations. In every experiment, the highest average is chosen to use in the final models.

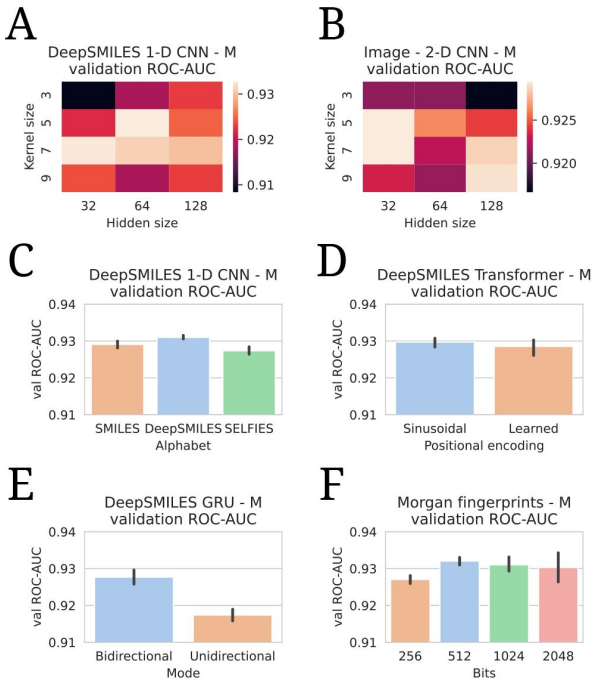

Figure 8.

ROC curve for best-performing model (Morgan Fingerprints drug embedder, Medium-sized spectrum embedder). The y-axis shows the average sensitivity (across patients), while the x-axis shows one minus the average specificity.

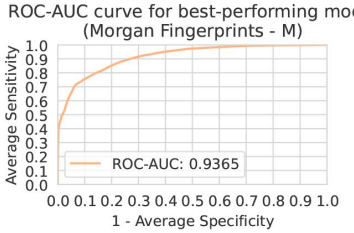

Figure 9.

Barplots showing test performance results for all trained models. Colors represent the different spectrum embedder model sizes. Performance is shown in terms of Macro ROC-AUC (computed per drug and averaged). Errorbars represent the standard deviation over five random seeds.

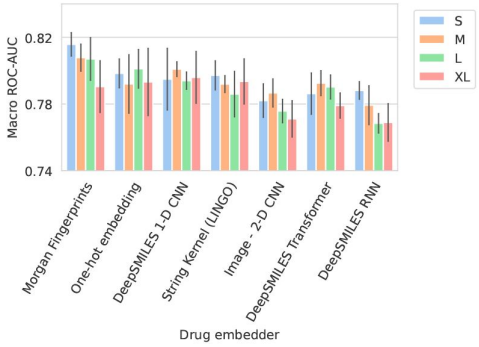

Figure 10.

Performance of models compared against a linear spectrum embedder baseline. The comparison is only shown for the best-performing drug embedder (Morgan Fingerprints). Errorbars represent the standard deviation over five random seeds.

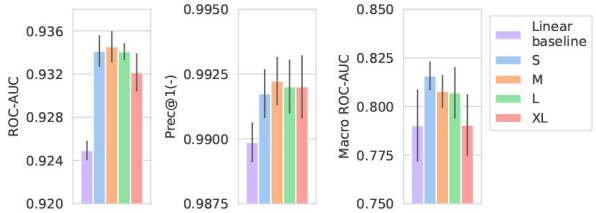

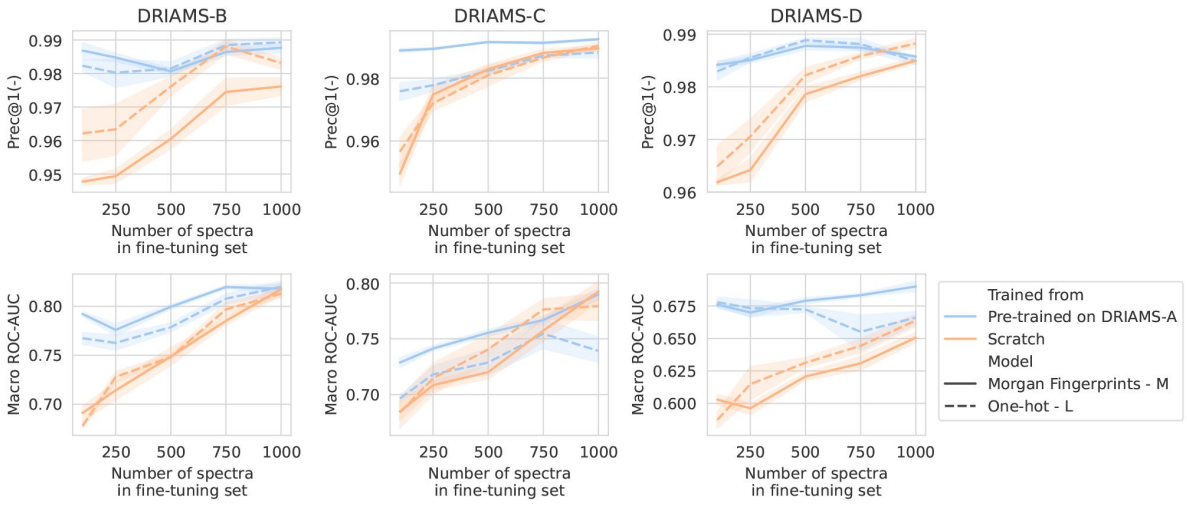

Figure 11.

Transfer learning of DRIAMS-A models to other hospitals. Errorbands show the standard deviation over five runs.

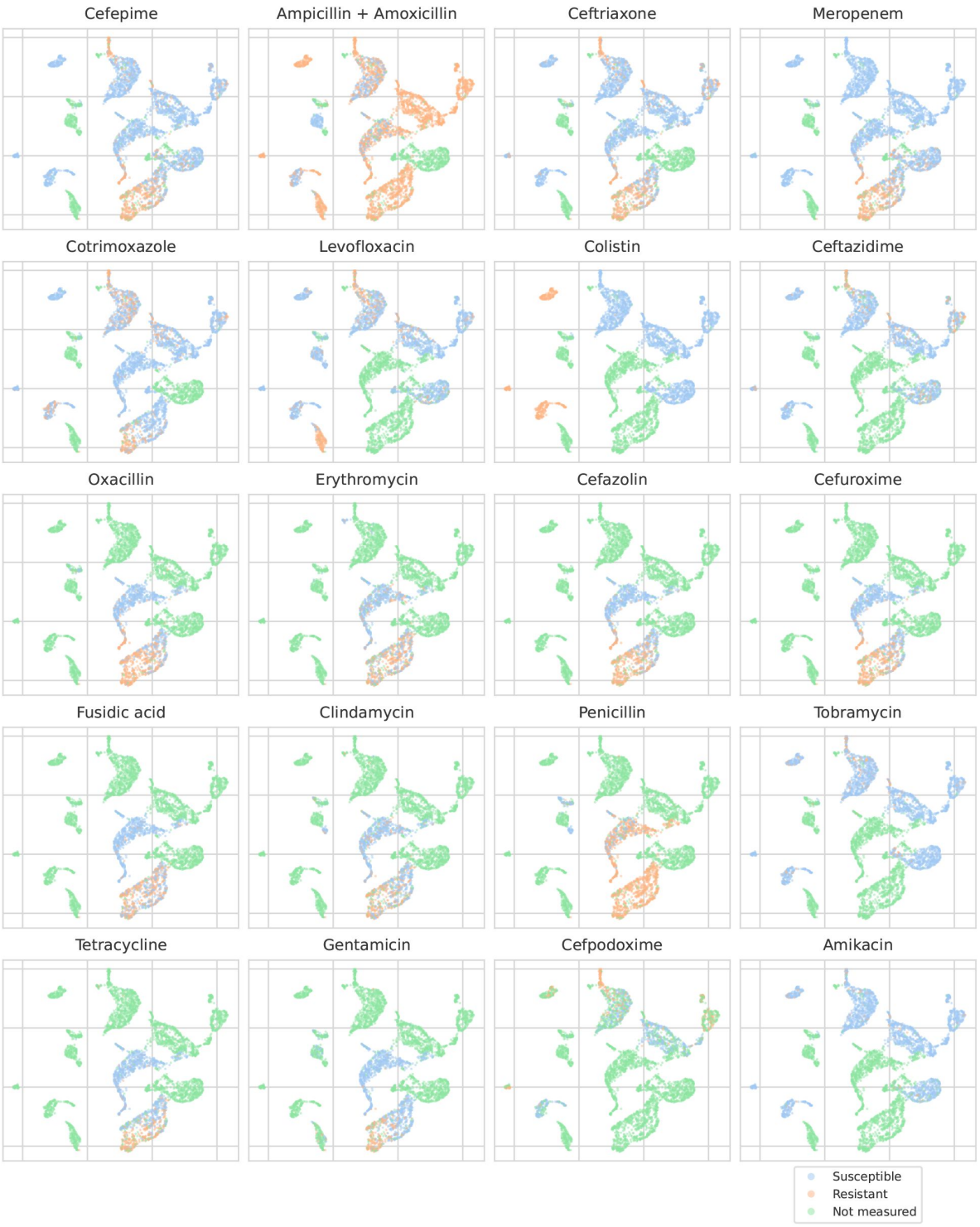

Figure 12.

UMAP scatterplots of test set MALDI-TOF spectra embeddings x_i. Embeddings from a "general" (trained on all spectra across species) recommender are shown. Only embeddings belonging to the 25 mostoccurring species in the test set are shown. Spectra are colored according to its AMR status to a certain drug. The twenty displayed drugs are selected based on a ranking of the product of the number of positive and negative labels $\sum_{i=1}^{n}[y_{ij}=0]\cdot\sum_{i=1}^{n}[y_{ij}=1]$. In this way, the drugs that have a lot of observed labels, both positives and negatives, are displayed. The drugs here are ranked 5-24 (the first four are shown in **Figure 4**). In order to map the clusters back to species, readers are referred back to **Figure 4**.

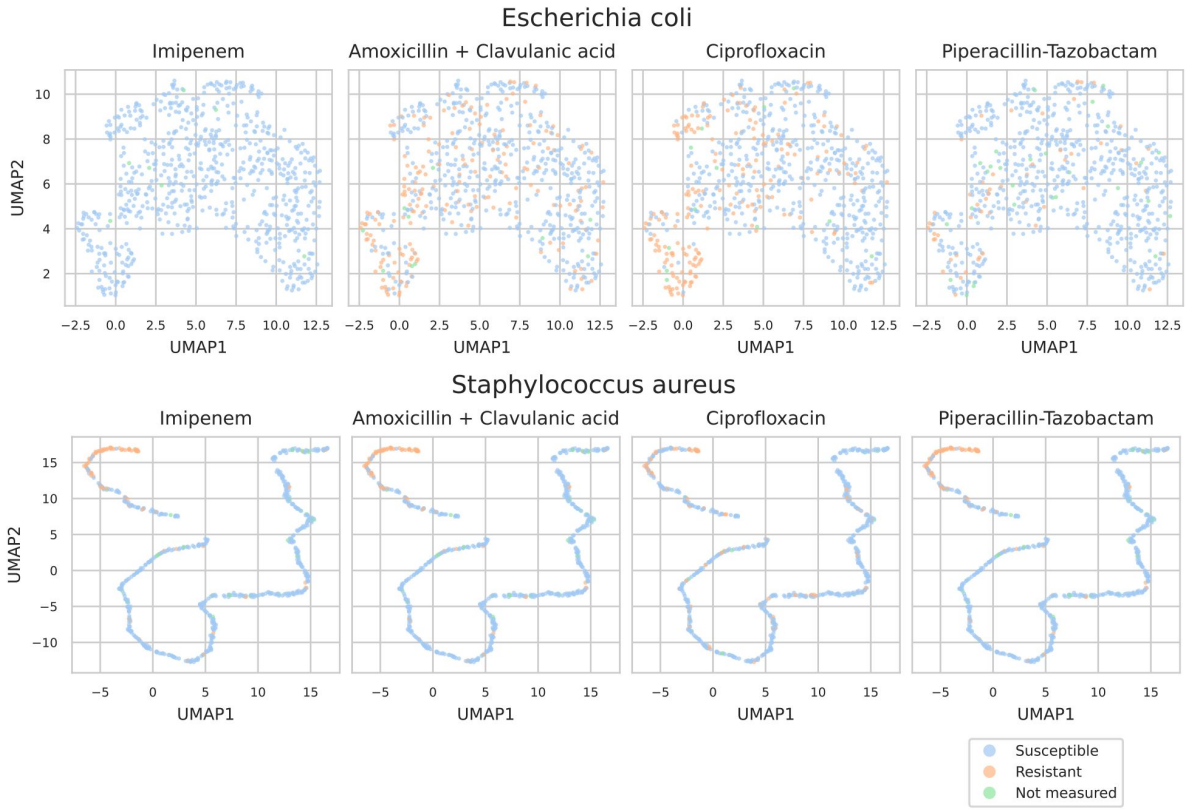

Figure 13.

UMAP scatterplots of test set MALDI-TOF spectra embeddings x_i. Embeddings from two "speciesspecific" recommenders are shown. Spectra are colored according to its AMR status to a certain drug.

corresponding with the splits used for the dual-branch experiments). The same preprocessed 6000-dimensional spectrum representations are used as input.

Logistic regression baselines are trained with the LBFGS solver for a maximum of 500 training iterations. For every species-drug combination, a grid search is performed on various hyperparameters, selecting the best based on validation ROC-AUC. The hyperparameters that are tuned are the scaling method on the features (either none, or standard scaling), and the L2 regularization strength ($c \in \{10^{-3}, 10^{-2}, \ldots, 10^{2}, 10^{3}\}$) For XGBoost, default parameters are used apart from those tuned. For every species-drug combina-tion, a grid is run, testing different numbers of trees (n_estimators ∈ {25, 50, 100, 200}) and learning rate (learning_rate ∈ {$10^{™3}$, 10^{-2}, 10^{-1}, 10^{0} }).

For the MLP baselines, the same hyperparameters are used as for the spectrum branch. Briefly recapitulated: between every two fully-connected layers, a series of operations consisting of (1) a GeLU activation, (2) a dropout rate of 0.2, and (3) layer normalization, is applied. The sizes of the models are as in **Table 1**, but then ending in 1 node instead of 64. For every speciesdrug combination, models are trained using the crossentropy loss and the Adam optimizer for a maximum of 250 epochs. A batch size of 128 is employed. A linear learning rate warm-up is applied over the first 250 steps. Early stopping based on validation ROC-AUC is applied with a patience of 10 epochs. The model with the best validation ROC-AUC during training is kept as final model. the best model out of four different learning rates (learning_rate ∈ {1e-5, 5e-5, 1e-4, 5e-4}) is chosen based on their validation ROC-AUC.

References

Hou Tsung-Yun, Chiang-Ni Chuan, Teng Shih-Hua (2019) **Current status of maldi-tof mass spectrometry in clinical microbiology** *Journal of food and drug analysis* **27**:404–414

Van Veen SQ, Claas ECJ, Kuijper Ed J (2010) **High-throughput identification of bacteria and yeast by matrix-assisted laser desorption ionization-time of flight mass spectrometry in conventional medical microbiology laboratories** *Journal of clinical microbiology* **48**:900–907

Cuénod Aline, Foucault Frédéric, Pflüger Valentin, Egli Adrian (2021) **Factors associated with maldi-tof mass spectral quality of species identification in clinical routine diagnostics** *Frontiers in Cellular and Infection Microbiology* **11**

Murray Christopher JL *et al.* (2022) **Global burden of bacterial antimicrobial resistance in 2019: a systematic analysis** *The Lancet* **399**:629–655

O'Neill Jim (2016) **Tackling drug-resistant infections globally: final report and recommendations**

Khan Zeeshan A, Siddiqui Mohd F, Park Seungkyung (2019) **Current and emerging methods of antibiotic susceptibility testing** *Diagnostics* **9**

Humphries Romney M (2022) **Ad hoc antimicrobial susceptibility testing from maldi-tof ms spectra in the clinical microbiology laboratory** *Clinical Chemistry* **68**:1118–1120

Weis Caroline, Horn Max, Rieck Bastian, Cuénod Aline, Egli Adrian, Borgwardt Karsten (2020) **Topological and kernel-based microbial phenotype prediction from maldi-tof mass spectra** *Bioinformatics* **36**:i30–i38

Weis Caroline *et al.* (2022) **Direct antimicrobial resistance prediction from clinical maldi-tof mass spectra using machine learning** *Nature Medicine* **28**:164–174

Shlaes David M *et al.* (1997) **Society for healthcare epidemiology of america and infectious diseases society of america joint committee on the prevention of antimicrobial resistance guidelines for the prevention of antimicrobial resistance in hospitals** *Infection Control & Hospital Epidemiology* **18**:275–291

Bai J, Fan ZC, Zhang LP, Xu XY, Zhang ZL (2017) **Classification of methicillin-resistant and methicillin-susceptible staphylococcus aureus using an improved genetic algorithm for feature selection based on mass spectra** *Proceedings of the 9th International Conference on Bioinformatics and Biomedical Technology* :57–63

Van Belkum Alex, Welker Martin, Erhard Marcel, Chatellier Sonia (2012) **Biomedical mass spectrometry in today's and tomorrow's clinical microbiology laboratories** *Journal of clinical microbiology* **50**:1513–1517

Dauwalder Olivier, Cecchini Tiphaine, Rasigade Jean Philippe, Vandenesch François (2023) **Matrix assisted laser desorption ionisation/time of flight (maldi/tof) mass spectrometry is not done revolutionizing clinical microbiology diagnostic** *Clinical Microbiology and Infection* **29**:127–129

Cao Yan, Wang Lei, Ma Ping, Fan Wenting, Gu Bing, Ju Shaoqing (2018) **Accuracy of matrix-assisted laser desorption ionization–time of flight mass spectrometry for identification of mycobacteria: a systematic review and meta-analysis** *Scientific reports* **8**:1–9

Vrioni Georgia, Tsiamis Constantinos, Oikonomidis George, Theodoridou Kalliopi, Kapsimali Violeta, Tsakris Athanasios (2018) **Maldi-tof mass spectrometry technology for detecting biomarkers of antimicrobial resistance: current achievements and future perspectives** *Annals of translational medicine* **6**

Florio Walter, Tavanti Arianna, Barnini Simona, Ghelardi Emilia, Lupetti Antonella (2018) **Recent advances and ongoing challenges in the diagnosis of microbial infections by maldi-tof mass spectrometry** *Frontiers in microbiology* **9**

Hettick Justin M, Kashon Michael L, Slaven James E, Ma Yan, Simpson Janet P, Siegel Paul D, Mazurek Gerald N, Weissman David N (2006) **Discrimination of intact mycobacteria at the strain level: a combined maldi-tof ms and biostatistical analysis** *Proteomics* **6**:6416–6425

Wang Hsin-Yao, Lee Tzong-Yi, Tseng Yi-Ju, Liu Tsui-Ping, Huang Kai-Yao, Chang Yung-Ta, Chen Chun-Hsien, Lu Jang-Jih (2018) **A new scheme for strain typing of methicillin-resistant staphylococcus aureus on the basis of matrix-assisted laser desorption ionization time-of-flight mass spectrometry by using machine learning approach** *PloS one* **13**

De Bruyne Katrien, Slabbinck Bram, Waegeman Willem, Vauterin Paul, De Baets Bernard, Vandamme Peter (2011) **Bacterial species identification from maldi-tof mass spectra through data analysis and machine learning** *Systematic and applied microbiology* **34**:20–29

Yu Jiaxin, Tien Ni, Liu Yu-Ching, Cho Der-Yang, Chen Jia-Wen, Tsai Yin-Tai, Huang Yu-Chen, Chao Huei-Jen, Chen Chao-Jung (2022) **Rapid identification of methicillin-resistant staphylococcus aureus using maldi-tof ms and machine learning from over 20,000 clinical isolates** *Microbiology Spectrum* **10**:e00483–22

Zhang Yu-Ming, Tsao Mei-Fen, Chang Ching-Yu, Lin Kuan-Ting, Keller Joseph Jordan, Lin Hsiu-Chen (2023) **Rapid identification of carbapenem-resistant klebsiella pneumoniae based on matrix-assisted laser desorption ionization time-of-flight mass spectrometry and an artificial neural network model** *Journal of Biomedical Science* **30**

Chung Chia-Ru, Wang Hsin-Yao, Yao Chun-Han, Wu Li-Ching, Lu Jang-Jih, Horng Jorng-Tzong, Lee Tzong-Yi (2023) **Data-driven two-stage framework for identification and characterization of different antibiotic-resistant escherichia coli isolates based on mass spectrometry data** *Microbiology Spectrum* :e03479–22

Mortier Thomas, Wieme Anneleen D, Vandamme Peter, Waegeman Willem (2021) **Bacterial species identification using maldi-tof mass spectrometry and machine learning techniques: A large-scale benchmarking study** *Computational and Structural Biotechnology Journal* **19**:6157–6168

Vervier Kévin, Mahé Pierre, Veyrieras Jean-Baptiste, Vert Jean-Philippe (2015) **Benchmark of structured machine learning methods for microbial identification from mass-spectrometry data** *arXiv*

Weis Caroline V, Jutzeler Catherine R, Borgwardt Karsten (2020) **Machine learning for microbial identification and antimicrobial susceptibility testing on maldi-tof mass spectra: a systematic review** *Clinical Microbiology and Infection* **26**:1310–1317

Visonà Giovanni, Duroux Diane, Miranda Lucas, Sükei Emese, Li Yiran, Borgwardt Karsten, Oliver Carlos (2023) **Multimodal learning in clinical proteomics: enhancing antimicrobial resistance prediction models with chemical information** *Bioinformatics* **39**

Waegeman Willem, Dembczyński Krzysztof, Hüllermeier Eyke (2019) **Multi-target prediction: a unifying view on problems and methods** *Data Mining and Knowledge Discovery* **33**:293–324

Iliadis Dimitrios, De Baets Bernard, Waegeman Willem (2022) **Multi-target prediction for dummies using two-branch neural networks** *Machine Learning* :1–34

He Xiangnan, Liao Lizi, Zhang Hanwang, Nie Liqiang, Hu Xia, Chua Tat-Seng (2017) **Neural collaborative filtering** *Proceedings of the 26th international conference on world wide web* :173–182

Zheng Lei, Noroozi Vahid, Yu Philip S (2017) **Joint deep modeling of users and items using reviews for recommendation** *Proceedings of the tenth ACM international conference on web search and data mining* :425–434

Radford Alec *et al.* (2021) **Learning transferable visual models from natural language supervision** *International conference on machine learning* :8748–8763

Chen Ting, Kornblith Simon, Norouzi Mohammad, Hinton Geoffrey (2020) **A simple framework for contrastive learning of visual representations** *In International conference on machine learning* :1597–1607

Karpukhin Vladimir, Oğuz Barlas, Min Sewon, Lewis Patrick, Wu Ledell, Edunov Sergey, Chen Danqi, Yih Wen-tau (2020) **Dense passage retrieval for open-domain question answering** *arXiv*

Lee Ingoo, Keum Jongsoo, Nam Hojung (2019) **Deepconv-dti: Prediction of drug-target interactions via deep learning with convolution on protein sequences** *PLoS computational biology* **15**

Lance Christopher *et al.* (2022) **Multimodal single cell data integration challenge: results and lessons learned** *bioRxiv* :2022–4

Yang Shu, Liu Xiaoxi, Ng Raymond T (2020) **Proberating: a recommender system to infer binding profiles for nucleic acid-binding proteins** *Bioinformatics* **36**:4797–4804

Beaumont Romain (2022) **Romain Beaumont. Clip retrieval: Easily compute clip embeddings and build a clip retrieval system with them. https://github.com/rom1504/clip-retrieval, 2022.**

Kim Sunghwan *et al.* (2023) **Pubchem 2023 update** *Nucleic acids research* **51**:D1373–D1380

Waegeman Willem, Dembczyński Krzysztof, Hüllermeier Eyke (2018) **Multi-target prediction: a unifying view on problems and methods** *Tutorial presented at ECML/PKDD 2018*

Rendle Steffen, Krichene Walid, Zhang Li, Anderson John (2020) **Neural collaborative filtering vs. matrix factorization revisited** *Proceedings of the 14th ACM Conference on Recommender Systems* :240–248

Vaswani Ashish, Shazeer Noam, Parmar Niki, Uszkoreit Jakob, Jones Llion, Gomez Aidan N, Kaiser ukasz, Polosukhin Illia (2017) **Attention is all you need** *Advances in neural information processing systems* **30**

Hendrycks Dan, Gimpel Kevin (2016) **Gaussian error linear units (gelus)** *arXiv*

Srivastava Nitish, Hinton Geoffrey, Krizhevsky Alex, Sutskever Ilya, Salakhutdinov Ruslan (2014) **Dropout: a simple way to prevent neural networks from overfitting** *The journal of machine learning research* **15**:1929–1958

Ba Jimmy Lei, Kiros Jamie Ryan, Hinton Geoffrey E (2016) **Layer normalization** *arXiv*

O'Boyle Noel, Dalke Andrew (2018) **Deepsmiles: an adaptation of smiles for use in machine-learning of chemical structures** *ChemRxiv*

Vidal David, Thormann Michael, Pons Miquel (2005) **Lingo, an efficient holographic text based method to calculate biophysical properties and intermolecular similarities** *Journal of chemical information and modeling* **45**:386–393

Kingma Diederik P, Ba Jimmy (2014) **Adam: A method for stochastic optimization** *arXiv*

Chen Tianqi, Guestrin Carlos (2016) **Xgboost: A scalable tree boosting system** *Proceedings of the 22nd acm sigkdd international conference on knowledge discovery and data mining* :785–794

Hüllermeier Eyke, Waegeman Willem (2021) **Aleatoric and epistemic uncertainty in machine learning: An introduction to concepts and methods** *Machine Learning* **110**:457–506

Lee Cecilia S, Lee Aaron Y (2020) **Clinical applications of continual learning machine learning** *The Lancet Digital Health* **2**:e279–e281

Capecchi Alice, Probst Daniel, Reymond Jean-Louis (2020) **One molecular fingerprint to rule them all: drugs, biomolecules, and the metabolome** *Journal of cheminformatics* **12**:1–15

Landrum Greg (2013) **Rdkit documentation** *Release* **1**

Weininger David (1988) **Smiles, a chemical language and information system. 1. introduction to methodology and encoding rules** *Journal of chemical information and computer sciences* **28**:31–36

Shazeer Noam (2020) **Glu variants improve transformer** *arXiv*

Liu Zhuang, Mao Hanzi, Wu Chao-Yuan, Feichtenhofer Christoph, Darrell Trevor, Xie Saining (2022) **A convnet for the 2020s** *Proceedings of the IEEE/CVF conference on computer vision and pattern recognition* :11976–11986

Cho Kyunghyun, Merriënboer Bart Van, Gulcehre Caglar, Bahdanau Dzmitry, Bougares Fethi, Schwenk Holger, Bengio Yoshua (2014) **Learning phrase representations using rnn encoder-decoder for statistical machine translation** *arXiv*

Öztürk Hakime, Ozkirimli Elif, Özgür Arzucan (2016) **A comparative study of smiles-based compound similarity functions for drug-target interaction prediction** *BMC bioinformatics* **17**:1–11

Krenn Mario, Häse Florian, Nigam AkshatKumar, Friederich Pascal, Aspuru-Guzik Alan (2020) **Self-referencing embedded strings (selfies): A 100% robust molecular string representation** *Machine Learning: Science and Technology* **1**

Devlin Jacob, Chang Ming-Wei, Lee Kenton, Toutanova Kristina (2018) **Bert: Pre-training of deep bidirectional transformers for language understanding** *arXiv*

Editors

Reviewing Editor
Lukas Folkman

Senior Editor
Wendy Garrett
Harvard T.H. Chan School of Public Health, Boston, United States of America

Reviewer #1 (Public Review):

Summary:

De Waele et al. reported a dual-branch neural network model for predicting antibiotic resistance profiles using matrix-assisted laser desorption/ionization time-of-flight (MALDI-TOF) mass spectrometry data. Neural networks were trained on the recently available DRIAMS database of MALDI-TOF mass spectrometry data and their associated antibiotic susceptibility profiles. The authors used dual branch neural network to simultaneously represent information about mass spectra and antibiotics for a wide range of species and antibiotic combinations. The authors showed consistent performance of their strategy to predict antibiotic susceptibility for different spectrum and antibiotic representations (i.e., embedders). Remarkably, the authors showed how small datasets collected at one location can improve the performance of a model trained with limited data collected at a second location. The authors also showed that species-specific models (trained in multiple antibiotic resistance profiles) outperformed both the single recommender model and the individual species-antibiotic combination models. Despite the promising results, the authors should explain in more detail some of the analyses reported in the manuscript (see weaknesses).

Strengths:

• A single AMR recommender system could potentially facilitate the adoption of MALDI-TOF based antibiotic susceptibility profiling into clinical practices by reducing the number of models to be considered, and the efforts that may be required to periodically update them.
• Authors tested multiple combinations of embedders for the mass spectra and antibiotics while using different metrics to evaluate the performance of the resulting models. Models trained using different spectrum embedder-antibiotic embedder combinations had remarkably good performance for all tested metrics. The average ROC AUC scores for global and species-specific evaluations were above 0.8.
• Authors developed species-specific recommenders as an intermediate layer between the single recommender system and single species-antibiotic models. This intermediate approach achieved maximum performance (with one type of the species-specific recommender achieving a 0.9 ROC AUC), outlining the potential of this type of recommenders for frequent

pathogens.
• Authors showed that data collected in one location can be leveraged to improve the performance of models generated using a smaller number of samples collected at a different location. This result may encourage researchers to optimize data integration to reduce the burden of data generation for institutions interested in testing this method.

Weaknesses:

• Section 4.3 ("expert baseline model"): the authors need to explain how the probabilities defined as baselines were exactly used to predict individual patient susceptible profiles.
• Authors do not offer information about the model features associated with resistance. Although I understand the difficulty of mapping mass spectra to specific pathways or metabolites, mechanistic insights are much more important in the context of AMR than in the context of bacterial identification. For example, this information may offer additional antimicrobial targets. Thus, authors should at least identify mass spectra peaks highly associated with resistance profiles. Are those peaks consistent across species? This would be a key step towards a proteomic survey of mechanisms of AMR. See previous work on this topic: PMIDs: 35586072 and 23297261.

https://doi.org/10.7554/eLife.93242.2.sa2

Reviewer #2 (Public Review):

The authors frame the MS-spectrum-based prediction of antimicrobial resistance prediction as a drug recommendation task. Weis et al. introduced the dataset this model is tested on and benchmark models which take as input a single species and are trained to predict resistance to a single drug. Instead here, a pair of drugs and spectrum are fed to 2 neural network models to predict a resistance probability. In this manner, knowledge from different drugs and species can be shared through the model parameters. Questions asked: 1. what is the best way to encode the drugs? 2. does the dual NN outperform the single spectrum-drug?

Overall the paper is well-written and structured. It presents a novel framework for a relevant problem.

https://doi.org/10.7554/eLife.93242.2.sa1

Author response:

The following is the authors' response to the previous reviews.

> ***Reviewer 1:***
>
> *• Although ROC AUC is a widely used metric. Other metrics such as precision, recall, sensitivity, and specificity are not reported in this work. The last two metrics would help readers understand the model's potential implications in the context of clinical research.*

In response to this comment and related ones by Reviewer 2, we have overhauled how we evaluate our models. In the revised version, we have removed Micro ROC-AUC, as this evaluation metric is hard to interpret in the recommender system setting. Instead, the updated version fully focuses on two metrics: ROC-AUC and Precision at 1 of the negative class, both computed per spectrum and then averaged (equivalent to the instance-wise metrics in the previous version of the manuscript). We believe these metrics best reflect the use-case of AMR recommenders. In addition, we have kept (drug-)macro ROC-AUC as a complementary evaluation metric. As the ROC-AUC can be decomposed into sensitivity and

specificity (at different prediction probability thresholds), we have added a ROC curve where sensitivity and specificity are indicated in Figure 8 (Appendices).

> *• The authors did not hypothesize or describe in any way what an acceptable performance of their recommender system should be in order to be adopted by clinicians.*

In Section 4.3, we have extended our experiments to include a baseline that represents a "simulated expert". In short, given a species, an expert can already make some best guesses as to what drugs will be effective or not. To simulate this, we count resistance frequencies per species and per drug in the training set, and use this as predictions of a "simulated expert".

We now mention in our manuscript that any performance above this level results in a real-world information gain for clinical diagnostic labs.

> *• Related to the previous comment, this work would strongly benefit from the inclusion of 1-2 real-life applications of their method that could showcase the benefits of their strategy for designing antibiotic treatment in a clinical setting.*

While we think this would be valuable to try out, we are an *in silico* research lab, and the study we propose is an initial proof-of-concept focusing on the methodology. Because of this, we feel a real-life application of the model is out-of-scope for the present study.

> *• The authors do not offer information about the model features associated with resistance. This information may offer insights about mechanisms of antimicrobial resistance and how conserved they are across species.*

In general, MALDI-TOF mass spectra are somewhat hard to interpret. Because of a limited body of work analyzing resistance mechanisms with MALDI-TOF MS, it is hard to link peaks back to specific pathways. For this reason, we have chosen to forego such an analysis. After all, as far as we know, typical MALDI-TOF MS manufacturers' software for bacterial identification also does not provide interpretability results or insights into peaks, but merely gives an identification and confidence score.

However, we do feel that the whole topic revolving around "the degree of biological insight a data modality might give versus actual performance and usability" merits further discussion. We have ultimately decided not to include a segment in our discussion section as it is hard to discuss this matter concisely.

> *• Comparison of AUC values across models lacks information regarding statistical significance. Without this information it is hard for a reader to figure out which differences are marginal and which ones are meaningful (for example, it is unclear if a difference in average AUC of 0.02 is significant). This applied to Figure 2, Figure 3, and Table 2 (and the associated supplementary figures).*

To make trends a bit more clear and easier to discern, in our revised manuscript, all models are run for 5 replicates (as opposed to 3 in the previous version).

There is an ongoing debate in the ML community whether statistical tests are useful for comparing machine learning models. A simple argument against them is that model runs are typically not independent from each other, as they are all trained on the same data. The assumptions of traditional statistical tests are therefore violated (t-test, Wilcoxon test, etc.). With such tests statistical significance of the smallest differences can simply be achieved by increasing the number of replicates (i.e. training the same models more times).

More complicated but more appropriate statistical tests also exist, such as the 5x2 cross-validated t-test of Dietterich: "Approximate statistical tests for comparing supervised classification learning algorithms", Neural computation 1998. However, these tests are typically not considered in deep learning, because only 10% of the data can be used for training, which is practically not desirable. The Friedman test of Demšar "On the appropriateness of statistical tests in machine learning." *Workshop on Evaluation Methods for Machine Learning in conjunction with ICML*. 2008., in combination with posthoc pairwise tests, is still frequently used in machine learning, but that test is only applicable in studies where many datasets are tested.

For those reasons, most deep learning papers that only analyse a few datasets typically do not consider any statistical tests. For the same reasons, we are also not convinced of the added value of statistical tests in our study.

> *• One key claim of this work was that their single recommender system outperformed specialist (single species-antibiotic) models. However, in its current status, it is not possible to determine that in fact that is the case (see comment above). Moreover, comparisons to species-level models (that combine all data and antibiotic susceptibility profiles for a given species) would help to illustrate the putative advantages of the dual branch neural network model over species-based models. This analysis will also inform the species (and perhaps datasets) for which specialist models would be useful to consider.*

We thank the reviewer for this excellent suggestion. In our new manuscript, we have dedicated an entire section of experiments to testing such species-specific recommender models (Section 4.2). We find that species-specific recommender systems generally outperform the models trained globally across all species. As a result, our manuscript has been majorly reworked.

> *• Taking into account that the clustering of spectra embeddings seemed to be species-driven (Figure 4), one may hypothesize that there is limited transfer of information between species, and therefore the neural network model may be working as an ensemble of species models. Thus, this work would deeply benefit from a comparison between the authors' general model and an ensemble model in which the species is first identified and then the relevant species recommender is applied. If authors had identified cases to illustrate how data from one species positively influence the results for another species, they should include some of those examples.*

See the answer to the remark above.

> *• The authors should check that all abbreviations are properly introduced in the text so readers understand exactly what they mean. For example, the Prec@1 metric is a little confusing.*

See the answer to a remark above for how we have overhauled our evaluation metrics in the revised version. In addition, in the revised version, we have bundled our explanations on evaluation metrics together in Section 3.2. We feel that having these explanations in a separate section will improve overall comprehensibility of the manuscript.

> *• The authors should include information about statistical significance in figures and tables that compare performance across models.*

See answer above.

> *• An extra panel showing species labels would help readers understand Figure 11.*

We have tried to play around with including species labels in these plots, but could not make it work without overcrowding the figure. Instead, we have added a reminder in the caption that readers should refer back to an earlier figure for species labels.

> *• The authors initially stated that molecular structure information is not informative. However, in a second analysis, the authors stated that molecular structures are useful for less common drugs. Please explain in more detail with specific examples what you mean.*

In the previous version of our manuscript, we found that one-hot embedding-based models were superior to structure-based drug embedders for general performance. The latter however, delivered better transfer learning performance.

In our new experiments however, we perform early stopping on “spectrum-macro” ROC-AUC (as opposed to micro ROC-AUC in the previous version). As a consequence, our results are different. In the new version of our manuscript, Morgan Fingerprints-based drug embedders generally outperform others both “in general” and for transfer learning. Hence, our previously conflicting statements are not applicable to our new results.

> *• The authors may want to consider adding a few sentences that summarize the 'Related work' section into the introduction, and converting the 'Related work' section into an appendix.*

While we acknowledge that such a section is uncommon in biology, in machine learning research, a “related work” section is very common. As this research lies on the intersection of the two, we have decided to keep the section as such.

> ***Reviewer 2:***
>
> *• Are the specialist models re-trained on the whole set of spectra? It was shown by Weis et al. that pooling spectra from different species hinders performance. It would then be better to compare directly to the models developed by Weis et al, using their splitting logic since it could be that the decay in performance from specialists comes from the pooling. See the section "Species-stratified learning yields superior predictions" in https://doi.org/10.1038/s41591-021-01619-9.*

We train our “specialist” (or now-called “species-drug classifiers”) just as described in Weis et al.: All labels for a drug are taken, and then subsetted for a single species. We have clarified this a bit better in our new manuscript. The text now reads:

“Previous studies have studied AMR prediction in specific species-drug combinations. For this reason, it is useful to compare how the dual-branch setup weighs up against training separate models for separate species and drugs. In Weis et al. (2020b), for example, binary AMR classifiers are trained for the following three combinations: (1) E. coli with Ceftriaxone, (2) K. pneumoniae with Ceftriaxone, and (3) S. aureus with Oxacillin. Here, such "species-drug-specific classifiers" are trained for the 200 most-common combinations of species and drugs in the training dataset.

> *• Going back to Weis et al. a high variance in performance between species/drug pairs was observed. The metrics in Table 2 do not offer any measurement of variance or statistical testing. Indeed, some values are quite close e.g. Macro AUROC of Specialist MLP-XL vs One-hot M.*

See our answer to a remark of Reviewer 1 for our viewpoint on statistical significance testing in machine learning.

> *• Since this is a recommendation task, why were no recommendation system metrics used, e.g. mAP@K, mRR, and so (apart from precision@1 for the negative class)? Additionally, since there is a high label imbalance in this task (~80% negatives) a simple model would achieve a very high precision@1.*

See the answer to a remark above for how we have overhauled our evaluation metrics in the revised version. In addition, in choosing our metrics, we wanted metrics that are both (1) appropriate (i.e. recommender system metrics), but also (2) easy to interpret for clinicians. For this reason, we have not included metrics such as mAP@K or mRR. We feel that "spectrum-macro" ROC-AUC and precision@1 cover a sufficiently broad evaluation set of metrics but are easy enough to interpret.

> *• A highly similar approach was recently published (https://doi.org/10.1093/bioinformatics/btad717). Since it is quite close to the publication date of this paper, it could be discussed as concurrent work.*

We thank the reviewer for bringing our attention to this study. We have added a paragraph in our revised version discussing this paper as concurrent work.

> *• It is difficult to observe a general trend from Figure 2. A statistical test would be advised here.*

See our answer to a remark of Reviewer 1 for our viewpoint on statistical significance testing in machine learning.

> *• Figure 5. UMAPs generally don't lead to robust quantitative conclusions. However, the analysis of the embedding space is indeed interesting. Here I would recommend some quantitative measures directly using embedding distances to accompany the UMAP visualizations. E.g. clustering coefficients, distribution of pairwise distances, etc.*

In accordance with this recommendation, we have computed many statistics on the MALDI-TOF spectra embedding spaces. However, we could not come up with any statistic that illuminated us more than the visualization itself. For this reason, we have kept this section as is, and let the figure speak for itself.

> *• Weis et al. also perform a transfer learning analysis. How does the transfer learning capacity of the proposed models differ from those in Weis et al?*

Weis et al. perform experiments towards "transferability", not actual transfer learning. In essence, they use a model trained on data from one diagnostic lab towards prediction on data from another. However, they do not conduct experiments to learn how much data such a pre-trained classifier needs to fine-tune it for adequate performance on the new diagnostic lab, as we do. The end of Section 4.4 discusses how our proposed models specifically shine in transfer learning. The paragraph reads:

"Lowering the amount of data required is paramount to expedite the uptake of AMR models in clinical diagnostics. The transfer learning qualities of dual-branch models may be ascribed to multiple properties. First of all, since different hospitals use much of the same drugs, transferred drug embedders allow for expressively representing drugs out of the box. Secondly, owing to multi-task learning, even with a limited number of spectra, a considerable fine-tuning dataset may be obtained, as all available data is "thrown on one pile"."

https://doi.org/10.7554/eLife.93242.2.sa0